



**University of  
Zurich<sup>UZH</sup>**

**Zurich Open Repository and  
Archive**

University of Zurich  
University Library  
Strickhofstrasse 39  
CH-8057 Zurich  
[www.zora.uzh.ch](http://www.zora.uzh.ch)

---

Year: 2018

---

## **Seasonal evolution of the subglacial hydrologic system modified by supraglacial lake drainage in western Greenland**

Andrews, Lauren C ; Hoffman, Matthew J ; Neumann, Thomas A ; Catania, Ginny A ; Lüthi, Martin P  
; Hawley, Robert L ; Schild, Kristin M ; Ryser, Claudia ; Morriss, Blaine F

**Abstract:** The impact of summer surface melt on Greenland Ice Sheet dynamics is modulated by the state of the subglacial hydrologic system. Studies of ice motion indicate that efficiency of the subglacial system increases over the melt season, decreasing the sensitivity of ice motion to surface melt inputs. However, the behavior of the subglacial hydrologic system is complex and some characteristics are still poorly constrained. Here we investigate the coevolution of subglacial hydrology and ice motion in the Pâkitsoq region of western Greenland during the 2011 melt season. We analyze measurements from 11 Global Positioning System stations, from which we derive ice velocity, longitudinal strain rates, and basal uplift, alongside observations of surface ablation and supraglacial lake drainages. We observe ice acceleration after the onset of local surface melting, followed by gradual ice deceleration, consistent with increasing subglacial efficiency. In the study area, supraglacial lake drainages cooccur with a change in regional strain rate patterns and ice deceleration, suggesting that lake drainages contribute to rapid subglacial reorganization. At lower ice surface elevations (below 900 m above sea level), ice motion is correlated with both total basal uplift and its rate of change, while at higher elevations (900–1,100 m above sea level), ice motion correlated only with the basal uplift rate. This pattern suggests that continued cavity growth or subglacial sediment dynamics may be important in the apparent increase in subglacial drainage efficiency at higher elevations in the ablation zone. Our results further suggest that transient subglacial behavior is important in the seasonal evolution of ice motion.

DOI: <https://doi.org/10.1029/2017jf004585>

Posted at the Zurich Open Repository and Archive, University of Zurich

ZORA URL: <https://doi.org/10.5167/uzh-162832>

Journal Article

Published Version

Originally published at:

Andrews, Lauren C; Hoffman, Matthew J; Neumann, Thomas A; Catania, Ginny A; Lüthi, Martin P; Hawley, Robert L; Schild, Kristin M; Ryser, Claudia; Morriss, Blaine F (2018). Seasonal evolution of the subglacial hydrologic system modified by supraglacial lake drainage in western Greenland. *Journal of Geophysical Research: Earth Surface*, 123(6):1479-1496.

DOI: <https://doi.org/10.1029/2017jf004585>

**RESEARCH ARTICLE**

10.1029/2017JF004585

**Key Points:**

- Ice velocity in Pákitsoq, western Greenland, exhibits clear signs of increased subglacial drainage efficiency over a melt season
- Supraglacial lake drainage events can be associated with inferred transitions between inefficient and efficient subglacial drainage
- Consistent with previous results, basal uplift rates are better correlated with horizontal ice velocity than total basal uplift

**Correspondence to:**

L. C. Andrews,  
lauren.c.andrews@nasa.gov

**Citation:**

Andrews, L. C., Hoffman, M. J., Neumann, T. A., Catania, G. A., Lüthi, M. P., Hawley, R. L., et al. (2018). Seasonal evolution of the subglacial hydrologic system modified by supraglacial lake drainage in western Greenland. *Journal of Geophysical Research: Earth Surface*, 123, 1479–1496. <https://doi.org/10.1029/2017JF004585>

Received 19 DEC 2017

Accepted 12 MAY 2018

Accepted article online 24 MAY 2018

Published online 30 JUN 2018

# Seasonal Evolution of the Subglacial Hydrologic System Modified by Supraglacial Lake Drainage in Western Greenland

Lauren C. Andrews<sup>1,2</sup> , Matthew J. Hoffman<sup>3</sup> , Thomas A. Neumann<sup>2</sup>, Ginny A. Catania<sup>4</sup> , Martin P. Lüthi<sup>5</sup> , Robert L. Hawley<sup>6</sup> , Kristin M. Schild<sup>6,7</sup> , Claudia Ryser<sup>8</sup>, and Blaine F. Morriss<sup>9</sup>

<sup>1</sup>Global Modeling and Assimilation Office, NASA Goddard Space Flight Center, Greenbelt, MD, USA, <sup>2</sup>Cryospheric Sciences Laboratory, NASA Goddard Space Flight Center, Greenbelt, MD, USA, <sup>3</sup>Fluid Dynamics and Solid Mechanics Group, Los Alamos National Laboratory, Los Alamos, NM, USA, <sup>4</sup>Jackson School of Geosciences, University of Texas at Austin, Austin, TX, USA, <sup>5</sup>Glaciology and Geomorphodynamics Group, Department of Geography, University of Zürich, Hanover, NH, USA, <sup>6</sup>Department of Earth Sciences, Dartmouth College, Zürich, Switzerland, <sup>7</sup>Now at Department of Earth Sciences, University of Oregon, Eugene, OR, USA, <sup>8</sup>Laboratory of Hydraulics, Hydrology and Glaciology, Swiss Federal Institute of Technology (ETH), Zürich, Switzerland, <sup>9</sup>Cold Regions Research and Engineering Laboratory, Hanover, NH, USA

**Abstract** The impact of summer surface melt on Greenland Ice Sheet dynamics is modulated by the state of the subglacial hydrologic system. Studies of ice motion indicate that efficiency of the subglacial system increases over the melt season, decreasing the sensitivity of ice motion to surface melt inputs. However, the behavior of the subglacial hydrologic system is complex and some characteristics are still poorly constrained. Here we investigate the coevolution of subglacial hydrology and ice motion in the Pákitsoq region of western Greenland during the 2011 melt season. We analyze measurements from 11 Global Positioning System stations, from which we derive ice velocity, longitudinal strain rates, and basal uplift, alongside observations of surface ablation and supraglacial lake drainages. We observe ice acceleration after the onset of local surface melting, followed by gradual ice deceleration, consistent with increasing subglacial efficiency. In the study area, supraglacial lake drainages cooccur with a change in regional strain rate patterns and ice deceleration, suggesting that lake drainages contribute to rapid subglacial reorganization. At lower ice surface elevations (below ~900 m above sea level), ice motion is correlated with both total basal uplift and its rate of change, while at higher elevations (~900–1,100 m above sea level), ice motion correlated only with the basal uplift rate. This pattern suggests that continued cavity growth or subglacial sediment dynamics may be important in the apparent increase in subglacial drainage efficiency at higher elevations in the ablation zone. Our results further suggest that transient subglacial behavior is important in the seasonal evolution of ice motion.

**Plain Language Summary** Each summer, the margins of the Greenland Ice Sheet experience intense surface melting. This meltwater is routed over the surface in supraglacial streams and stored in supraglacial lakes, but eventually reaches the bed of the ice sheet via crevasses and moulins. The interaction between this meltwater and the overlying ice causes changes to the subglacial hydrologic system, which subsequently causes changes in ice motion. Here we use measurements from 11 Global Positioning System stations, alongside observations of surface melt rates and supraglacial lake drainages, to improve our understanding of the subglacial hydrologic system. In our study area, supraglacial lake drainages tend to cooccur with slowdowns in ice motion, suggesting that the rapid drainage of these large volumes of water can alter the subglacial hydrologic system, allowing it to more readily transmit meltwater. Our observations also indicate that at high elevations, the seasonal pattern of ice motion is controlled by small changes over large regions, either in sediments or in pockets of water on the downstream side of bedrock bumps, not necessarily by the formation of large subglacial channels. These findings suggest that current models of the subglacial system need modifications to include the physics associated with supraglacial lake drainages and small-scale processes.

## 1. Introduction

The routing of summer meltwater to the ice sheet bed influences ice flow of Greenland Ice Sheet (GrIS) marginal regions (e.g., Hoffman et al., 2011; van de Wal et al., 2008; Zwally et al., 2002). Seasonally produced meltwater, delivered via crevasses and moulins, overwhelms the winter subglacial hydrologic system, increasing subglacial water pressure and basal sliding rates, consequently accelerating aggregate ice flow (Bartholomew

et al., 2010; Hoffman et al., 2011; Iken & Bindshadler, 1986; Nienow et al., 1998). The continued production and delivery of meltwater to the bed gradually encourages formation of efficient subglacial channels (e.g., Bartholomew et al., 2010; Schoof, 2010) and evolution of inefficient and weakly connected components of the subglacial system (Andrews et al., 2014; Hoffman et al., 2016; Hoffman & Price, 2014; Meierbachtol et al., 2013). This subglacial evolution causes a decline in regional subglacial pressure and deceleration of late summer and autumn ice motion, which can mitigate high early-summer ice speeds (Sole et al., 2013; Tedstone et al., 2013, 2015).

The evolution of the subglacial system can cause a multiyear deceleration of ice velocity near the margin of land-terminating regions of the GrIS, despite increasing surface meltwater production (Stevens et al., 2016; Tedstone et al., 2015). However, at high elevations, this multiyear decline in ice velocity is absent or reversed (Doyle et al., 2014; Tedstone et al., 2015). This contrasting ice-velocity response to meltwater input is thought to be due to the rate and extent of subglacial channelization (Doyle et al., 2014). Because the development of subglacial channels is driven primarily by melting of the overlying ice caused by the turbulent dissipation of heat, the low bed and surface slopes at higher elevations may limit the formation of efficient subglacial channels even with substantial surface melt input (Chandler et al., 2013; Dow et al., 2015; Meierbachtol et al., 2013). Consequently, in the absence of channels, the state of inefficient and weakly connected regions of the bed or flow coupling may govern ice motion (Andrews et al., 2014; Hoffman et al., 2016; Meierbachtol et al., 2013; Price et al., 2008), limiting the maximum efficiency of the subglacial system and the observed late-season slow down.

Despite extensive study of ice sheet hydrology, questions still remain regarding how various controls, including supraglacial water flow and subglacial characteristics, modulate the evolution of the subglacial system (e.g., Nienow et al., 2017). Recent modeling suggests that supraglacial lakes will become more spatially extensive (Ignéczi et al., 2016; Leeson et al., 2015), yet the impact of cascading lake drainages on subglacial evolution and subsequent ice flow is poorly understood, partly due to their infrequent inclusion in subglacial models (Fitzpatrick et al., 2014; Williamson et al., 2017). Furthermore, limits on subglacial channelization at moderate to higher ice sheet elevations—and the subsequent role of inefficient types of subglacial drainage on seasonal ice velocity evolution—are constrained only by relatively limited observational and modeling evidence (Andrews et al., 2014; Hoffman et al., 2016; Meierbachtol et al., 2013).

Here we analyze ice velocity longitudinal strain rate gradients, and basal uplift derived from Global Positioning System (GPS) positions, in conjunction with surface melt rates and supraglacial lake drainages, to determine how ice velocity responds to inferred changes in the subglacial drainage system in the Pâkitsoq region of western Greenland during the 2011 summer melt season. We find that the transition between inefficient and efficient subglacial drainage can be modulated by the timing of cascading supraglacial lake drainages within our study area and, at higher elevations, this transition may not be related to increasing subglacial channelization. Instead, it occurs, at least in part, due to increasing drainage efficiency elsewhere within the subglacial system.

## 2. Materials and Methods

### 2.1. Field Location

We deployed 11 GPS stations and two weather stations within the Sermeq Avannarleq catchment, north of Jakobshavn Isbræ, to constrain the seasonal evolution of surface melt and ice motion (Figure 1a). Surface ice speeds in this region range between 60 and 140 m/year (0.15 and 0.4 m/day), and bed topography is complex, with overdeepenings that may host extensive subglacial sediments (Figures 1b and 1c; Andrews et al., 2014; Hoffman et al., 2011; Joughin et al., 2010, 2016; Walter et al., 2014).

GPS station names reflect the distance from the Sermeq Avannarleq terminus and the distance north or south of the flow line, except for FOXX, GULL, and HARE, which include weather stations. These GPS stations fall between 600 and 1,100 m above sea level (asl), similar to previous low- and moderate-elevation GPS stations, boreholes, and dye tracing experiments located at Russell Glacier (e.g., Bartholomew et al., 2011; Chandler et al., 2013; van de Wal et al., 2015; Wright et al., 2016). Therefore, we generally characterize GPS stations below 900 m asl as low elevation (19N1, FOXX, 22N4, 25N1, and GULL) and stations at elevations between 900 and 1,100 m asl as moderate elevation (28N4, 33N1, HARE, 37N4, 38S3, and 41N1).

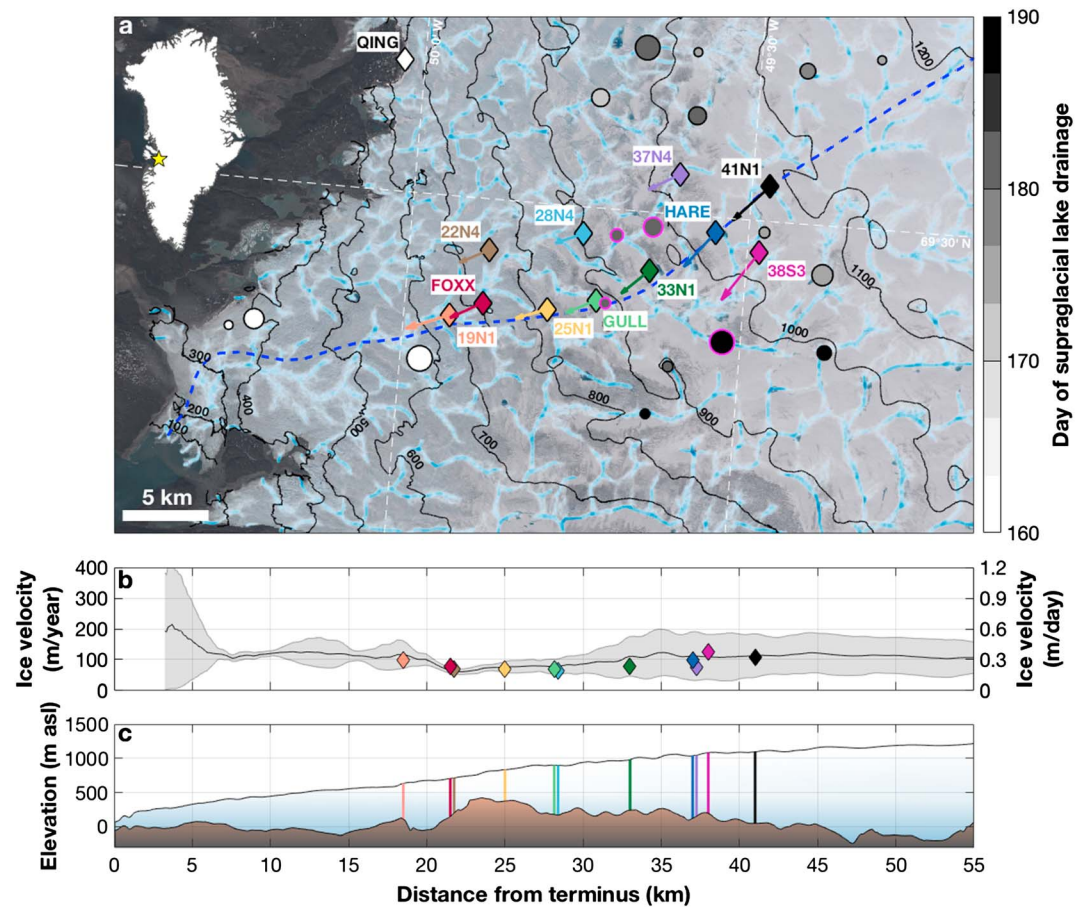


**Figure 1.** Landsat-8 optical image from July 2013 with locations of GPS stations (diamonds), background ice flow direction (arrows) along the Sermeq Avannarleq flow line (blue dashed line), supraglacial lake drainages (grey circles, scaled by maximum surface area; Morriss et al., 2013), potential subglacial flow paths (blue, intensity scales to the probability that water will flow along a given path for a range of subglacial water pressures; Andrews, 2015), and ice surface elevation contours (black lines, 100-m contour interval; Howat et al., 2014). Inset indicates the location of the study area (yellow star). (b) Winter background flow velocities derived from GPS (diamonds) and InSAR (black line with grey error bars; Joughin et al., 2010, 2016). (c) GPS locations (vertical lines colored as in (a) and (b)) and ice surface (Howat et al., 2014, 2015) and subglacial topography along flow line (Morlighem et al., 2014, 2015).

## 2.2. Supraglacial Melt Supply

We monitored meteorological conditions (air temperature and pressure, wind speed and direction, humidity, and precipitation) every 30 min at the FOXX and HARE GPS stations using Vaisala WTX520 weather transmitters between May and September 2011. Additional weather stations at FOXX and GULL (installed in July 2011) and one permanent GC-Net station, JAR-2 (69.415°N, 50.093°W, 507 m asl; Steffen et al., 1996) recorded more complete radiative observations, including shortwave and longwave radiation and surface ablation, on either 5-min (FOXX and GULL) or 1-hr (JAR-2) intervals.

As surface-melt measurements are only collected at FOXX and GULL field sites after mid-July 2011, we choose to model 6-hr mean surface melt for the entire 2011 melt season using a modified degree-index model that includes incoming shortwave radiation and ice-surface albedo (Pellicciotti et al., 2005). Following Pellicciotti et al. (2005), we calculate 6-hr mean surface melt, where surface melt,  $S_m$ :

$$S_m = \begin{cases} B_t T + B_{sw}(1 - \alpha)SW, & T > T_m \\ 0, & T \leq T_m \end{cases} \quad (1)$$

where  $T$  is the mean daily air temperature at each site,  $T_m$  is the freezing temperature (0 °C),  $\alpha$  is the ice-surface albedo, and  $SW$  is the incoming solar radiation. For  $\alpha$ , we use the MOD10A1 daily surface-albedo

product Moderate-Resolution Imaging Spectroradiometer (MODIS), which has a resolution of 500 m (Hall et al., 2006) and has been validated previously over our study area (Stroeve et al., 2006). Where MODIS  $\alpha$  exceeds 2 standard deviations of its 11-day mean or there is no data due to cloud cover, the 11-day median  $\alpha$  is used, following Box et al. (2012).  $SW$  varied minimally across the study area; therefore, we represent  $SW$  over the study area with JAR-2 measurements.  $B_t$  and  $B_{sw}$  are empirical coefficients for melt sensitivity.

We determined surface melting in three steps. First, we calibrated  $B_t$  and  $B_{sw}$  using observed  $S_m$ ,  $T$ , and  $SW$  at JAR2 and local MODIS  $\alpha$  value between day 135 and 265 of 2011. Multivariate regression returns values of 2.29 and 0.015 for  $B_t$  and  $B_{sw}$ , respectively. Next, we calculated 6-hr surface melt at FOXX, GULL, and HARE using the calibrated melt-sensitivity coefficients. Because air temperatures were not recorded at GULL before July, we estimated early season  $T$  at GULL using the time varying lapse rate between FOXX and HARE between day 140 and day 210. Finally, we validated the modeled melt at FOXX and GULL using measured surface ablation. When compared to observed surface melt at FOXX and GULL, 6-hr surface melt modeled using equation (1) exhibits a root-mean-square error of 10.8 mm and a bias of  $-0.01$  mm. Incorporation of incoming solar radiation and surface albedo improves (reduces) the root-mean-square error and model bias between modeled and measured surface ablation by 1.7 and 0.01 mm, respectively, relative to a temperature only index model ( $B_t = 2.87$ ). This improvement arises primarily during the latter part of the summer melt season when  $SW = 0$  for parts of the day.

In addition to surface melt that routes directly to the bed within hours, drainages of supraglacial lakes also perturb ice velocity within our study area. Therefore, we also analyze the location, timing, and size of supraglacial lake drainages identified previously within our study area during the 2011 melt season (Figure 1a; Morriss et al., 2013).

### 2.3. Ice Motion

We recorded surface displacement at 11 locations along Sermeq Avannarleq using a series of high precision, L1/L2 GPS stations (Figure 1a). A bedrock base-station (QING) was also established during the observation period as a fixed reference station for differential processing of the GPS observables. Positions were recorded by a mix of Trimble NetR5 (FOXX, HARE, and 37N4), NetR8 (GULL and QING), and R7 (19N1, 22N4, 25N1, 28N4, 33N1, 38S3, and 41N1) receivers with Trimble Zephyr Geodetic 2 antennas.

On-ice GPS stations followed previous station design and installation procedures to accommodate substantial surface ablation, high winds, and extended periods of darkness (e.g., Anderson et al., 2004; Hoffman et al., 2011). GPS receivers logged positions continuously at 15-s intervals during the summer melt season; however, poor satellite configuration and power failure resulted in some data gaps. GPS station 28N4 failed after day 190.

On-ice kinematic GPS positions were determined using carrier-phase differential processing relative to the bedrock mounted reference station (QING; baselines between 15 and 24 km to on-ice stations) using Track v1.24 (Chen, 1998) and final International GNSS Service satellite orbits following techniques described by Hoffman et al. (2011) and Andrews et al. (2014). The relative position of each on-ice station was determined at 15-s intervals. As part of processing, kinematic station motion was constrained on an epoch-by-epoch basis to 2,000 m/year to permit rapid, short-term velocity changes. The mean uncertainty of the 15-s positions is 4 mm in the horizontal and 6 mm in the vertical. After Track (i.e. the software) processing, each 15-s time series of on-ice station position was smoothed with a 6-hr phase-preserving filter to eliminate spurious signals associated with GPS uncertainties, and then decimated to 15-min time series. The smoothed positions were used to calculate 6-hr and 24-hr velocities using a centered time window to limit aliasing that may result from using discrete time intervals. Calculated 24-hr velocities have a mean uncertainty of  $\sim 4$  m/year; for 6-hr velocities, this uncertainty is  $\sim 9$  m/year.

### 2.4. Strain Rates

Longitudinal and lateral strain rates describe the spatial gradients of ice motion in the along-flow and across-flow directions, respectively. Here we use the change in distance between two GPS station positions,  $\Delta L_{ij}$ , in the along-flow (subscript  $xx$ ) and across-flow (subscript  $yy$ ) directions over a given time interval,  $\Delta t$ , to calculate longitudinal and lateral strain rates:

$$\dot{\epsilon}_{ij} = \frac{\Delta L_{ij}}{L_{0,ij} \Delta t}, \quad i = xx, yy \quad (2)$$



**Table 1**  
Characteristics of GPS Stations Used in Ice Velocity, Strain Rate, and Basal Uplift Calculations

Station	Longitudinal baseline length (m)	Along-flow endpoints	Lateral baseline length (m)	Across-flow endpoints	Mean ice thickness (m) <sup>a</sup>	Mean surface elevation (m) <sup>a</sup>
FOXX	1993.64	19N1, FOXX	3081.08	FOXX, 22N4	693	677
25N1	3778.35	FOXX, 25N1	3081.08	FOXX, 22N4	606	770
GULL	2783.12	25N1, GULL	3909.67	GULL, 28N4	505	867
33N1	3551.42	GULL, 33N1	3909.67	GULL, 28N4	718	941
HARE	4418.51	33N1, HARE	6378.65	38S3, 37N4	735	1014
41N1	4133.13	HARE, 41N1	6378.65	38S3, 37N4	888	1071

<sup>a</sup>Mean ice thickness and surface elevation between along-flow end points from Morlighem et al. (2014, 2015).

where  $L_{0,ij}$  is the initial baseline distance between the two stations and taken to be the distance on day 150, before the onset of surface melting (Table 1), and  $\Delta t$  is 24 hr.

We quantify the uncertainty in horizontal strain rates,  $\delta \dot{\epsilon}_{ij}$ , following Hoffman et al. (2011) and Howat et al. (2008):

$$\delta \dot{\epsilon}_{ij} = \sqrt{2} \eta (L_{ij} \Delta t)^{-1} \quad (3)$$

where  $\eta$  is the uncertainty in the baseline distance between stations, which we calculate from the 1-sigma positional uncertainty of each station. This uncertainty is propagated through all calculations.

We calculate longitudinal strain rates between each pair of adjacent stations along the primary ice flow line, yielding six unique time series. We calculate lateral strain rates between FOXX and 22N4, GULL and 28N4, and HARE and 37N4. Lateral strain rates in our study area have less variability than longitudinal strain rates; therefore, when calculating vertical strain rates, we use the lateral strain rate measurement nearest to each longitudinal strain rate measurement (Table 1). GPS 28N4 failed on day 190, truncating both the velocity record and lateral strain rate time series there. For the remainder of the melt season, we represent the lateral strain rate between GULL and 28N4 as the mean of the calculated strain rate between days 140 and 190.

Assuming ice is incompressible, we approximate the vertical strain rate,  $\dot{\epsilon}_{zz}$ , using continuity:

$$\dot{\epsilon}_{zz} = -(\dot{\epsilon}_{xx} + \dot{\epsilon}_{yy}) \quad (4)$$

Uncertainty in the vertical strain rate is calculated by propagating the uncertainty in the along- and across-flow strain rates through equation (4).

To examine how longitudinal strain rates change over the course of the melt season, we determine the strain rate anomaly relative to the mean winter background strain rate values (calculated between days 140 and 150). We linearly interpolate these data along the flow line to evaluate the spatial variability of strain rate anomalies.

## 2.5. Basal Uplift

Basal uplift is a proxy for cavity opening and/or sediment dilation at the bed of the ice sheet and is generally inferred to be representative of subglacial water storage (e.g., Anderson et al., 2004; Mair et al., 2002; Sugiyama & Gudmundsson, 2004). On hard-bedded glaciers, basal uplift is thought to be the result of subglacial cavity growth; on soft-bedded glaciers, basal uplift may be a combination of sediment dilation and cavity opening, which cannot yet be disentangled (e.g., Howat et al., 2008). Our field area likely contains both hard and soft bedded regions (Walter et al., 2014), so we use the more general term “basal uplift” instead of bed separation.

To isolate basal uplift, we remove vertical strain (equation (4)) and bed-parallel motion from total GPS-derived vertical motion,  $w_s$ , following common procedures (Anderson et al., 2004; Harper et al., 2007; Hoffman et al., 2011; Howat et al., 2008; Mair et al., 2002; Sugiyama & Gudmundsson, 2004), where:

$$w_s = u_b \tan \theta + \dot{\epsilon}_{zz} H + \dot{c} \quad (5)$$

The first term on the right-hand side of the equation is bed parallel motion, where  $u_b$  is horizontal sliding at the ice-bed interface and  $\theta$  is the local bed slope. The second term on the right is the thickness-integrated vertical strain rate, where  $H$  is ice thickness and  $\dot{\epsilon}_{zz}$  is the vertical strain rate, which we assume to be depth-invariant following previous work (Anderson et al., 2004; Hoffman et al., 2011; Howat et al., 2008). Vertical strain rate does vary with depth (e.g., Ryser, Lüthi, Andrews, Hoffman, et al., 2014), but it is reasonably represented by the surface value at FOXX and GULL, so we keep the assumption of depth invariance in order to maintain consistency across all basal uplift calculations. The last term on the right-hand-side of equation (5),  $\dot{c}$ , is the rate of cavity opening, that is, basal uplift.

We estimate the bed-parallel motion as a residual from winter background conditions (days 140–150, indicated by the subscript  $bg$ ), during which time we assume that the components of bed-parallel motion and vertical strain are constant and the basal uplift rate is zero:

$$u_{b,bg} \tan \theta = w_{s,bg} - \dot{\epsilon}_{zz,bg} H \quad (6)$$

As the total horizontal displacement of the GPS stations over the summer melt season is small ( $<100$  m), we assume that the bed slope is constant during our observation window (days 140–260).

We then integrate equation (5) to calculate displacement due to basal uplift,  $\dot{c}\Delta t$ :

$$\dot{c}\Delta t = \Delta z_s - \left( \frac{u_s}{u_{s,bg}} \right) u_{b,bg} \tan \theta - \dot{\epsilon}_{zz} H \Delta t \quad (7)$$

where the GPS-derived vertical displacement is indicated by  $\Delta z_s$  and the subscript  $s$  denotes a surface measurement. We make the conservative assumption that  $u_s, bg = u_{b, bg}$  following Hoffman et al. (2011) and note that during the summer melt season, basal sliding in at FOXX and GULL accounts for up to 90% of observed surface motion (Ryser, Lüthi, Andrews, Hoffman, et al., 2014).

Basal uplift is a time integral and thus depends on how periods of no data are treated. We linearly interpolate basal uplift rates during periods of missing data, but we mask these periods when presenting the results. This linear interpolation causes slight differences in the total magnitude of basal uplift compared with other gap-filling methods, but it does not influence the trend over the melt season nor does it substantially influence the relative magnitude of basal uplift.

### 3. Results

#### 3.1. Horizontal Ice Flow

All GPS stations exhibited seasonal motion consistent with previous observations within the Pâkitsoq region and elsewhere in Greenland (Figures 2 and 3; e.g., Bartholomew et al., 2010; Hoffman et al., 2011). The time between the onset of melting and observed ice acceleration increased with increasing distance from the terminus. At low elevations, ice acceleration began three to five days after the onset of persistent surface melting occurred (day  $\sim 160$  for stations 19N1, FOXX, and 22N4 and day  $\sim 163$  for stations GULL, 28N4, and 33N1; Figures 2a and 2b). At HARE, 37N4, 38S3, and 41N1, ice acceleration began  $\sim 11$  days after melt onset, on day  $\sim 168$  (Figure 2c).

The transition to gradual ice deceleration was temporally associated with identified lake drainage events on day  $\sim 182$  for stations below GULL and day  $\sim 188$  for GULL and moderate elevations (Figure 2). In all instances, ice velocity fell below spring background values before the end of the melt season, with low-elevation velocity falling below this point at day  $\sim 210$  and moderate elevation stations at day  $\sim 223$ . Ice velocity continued to decline until day  $\sim 235$ , when a precipitation and melt event spurred widespread acceleration for approximately six days (Doyle et al., 2015).

The seasonal pattern of ice motion is overlain by additional acceleration events related to both diurnal and event-type surface melt and supraglacial lake drainages (Figure 3). Diurnal variations in ice velocity occurred at all GPS stations, with the daily range generally proportional to daily surface melt production. Stations generally experienced the onset of strong diurnal variations in velocity with the onset of ice acceleration, though they tend to be small for stations above  $\sim 1,000$  m asl.

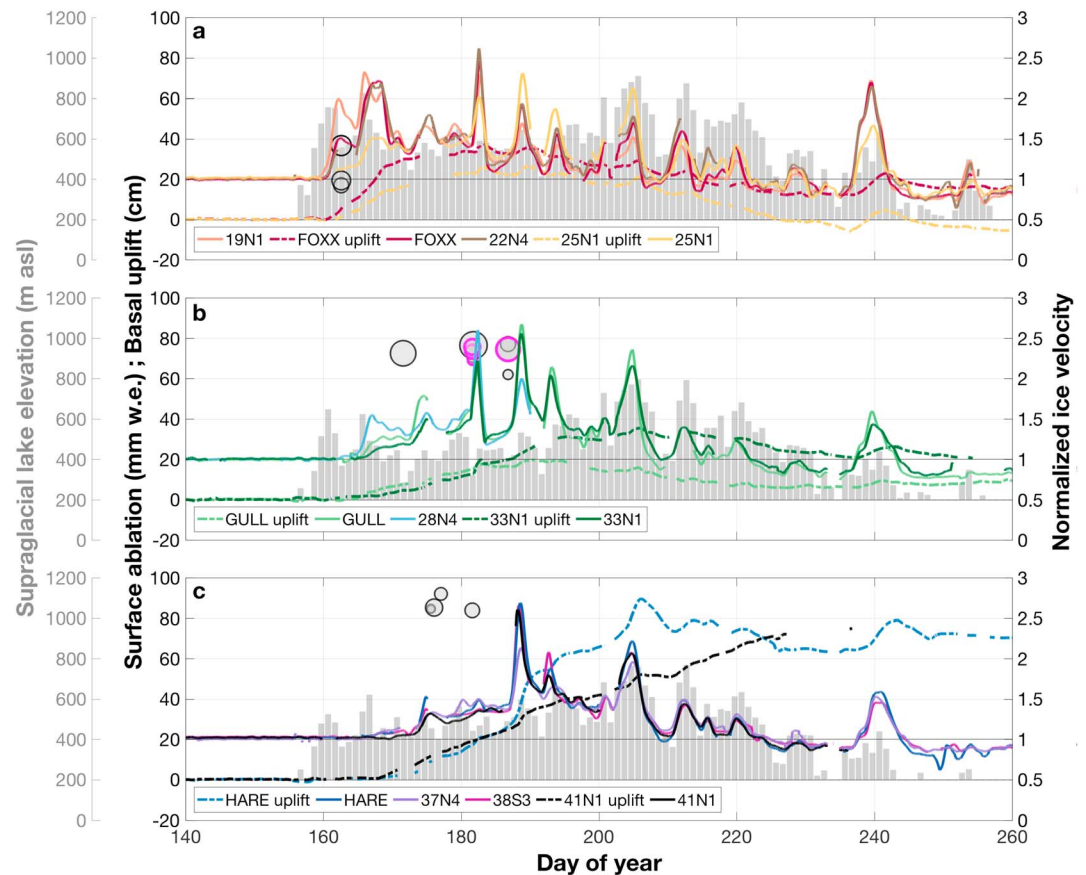


**Figure 2.** The 24-hr GPS-derived ice velocity divided by winter background values (solid lines), basal uplift measurements (dashed lines), daily modeled surface ablation (grey bars), and supraglacial lake drainages (grey circles) for 2011. Lakes that drained within or impacted the velocities of the GPS network are outlined in magenta. (a) GPS stations with surface elevations between 600–850 m asl and lake drainages below 850 m asl (b) GPS stations and lake drainages with surface elevations between 850–1,000 m asl (c) GPS stations with surface elevations between 1,000 and 1,100 m asl and lake drainages between 1,000 and 1,200 m asl.

In the Pákitsoq region, there are 20 lake drainages during 2011, which occur in six different clusters (Morris et al., 2013). Two of these lake drainage clusters included events that resulted in short-term accelerations of more than 200% of winter background speeds (Figure 3). According to remote-sensing observations, the first lake-drainage event occurred when three lakes within the GPS network drained on day  $181.6 \pm 2$  (Morris et al., 2013) and precipitated some of the highest recorded velocities in our study area (Figure 3). Using GPS observations, we can more tightly constrain the timing of these lake drainages and examine their propagation through the subglacial system. Initial rapid acceleration was observed at 33N1 starting on day 182 at approximately 02:24 UTC and was caused by the drainage of two lakes just north of 33N1. Peak “lake drainage” speed occurred at 10:15 UTC on day 182. This peak speed then propagated downstream from 33N1 to 28N4 (10:45 UTC), GULL (12:30 UTC), 22N4 (14:46 UTC), 25N1 (16:14 UTC), FOXX (16:45 UTC), and finally at 19N1 (18:44 UTC). GULL had a more muted velocity response and is located on a branch of the predicted subglacial drainage path within Sermeq Avannarleq, suggesting that the propagation of the meltwater from the first two lake drainages induced stresses that triggered the drainage at GULL (Hoffman et al., 2018). Station 25N1 also has a more muted velocity response, potentially due its location relative to modeled subglacial flow paths. Overall, the observed pattern of the acceleration front corresponds well with the modeled subglacial flow paths (Figure 1a).

The second lake-drainage event is not as well constrained. However, remote-sensing observations indicate three lake drainages, one large and two small, on day  $186.8 \pm 2.8$  (Morris et al., 2013). GPS observations suggest that the drainage event was initially observed at 41N1 on day 187 at approximately 13:25 UTC and peak velocity was reached on day 188 at 02:15 UTC. This velocity pattern then propagated downstream to 38S3



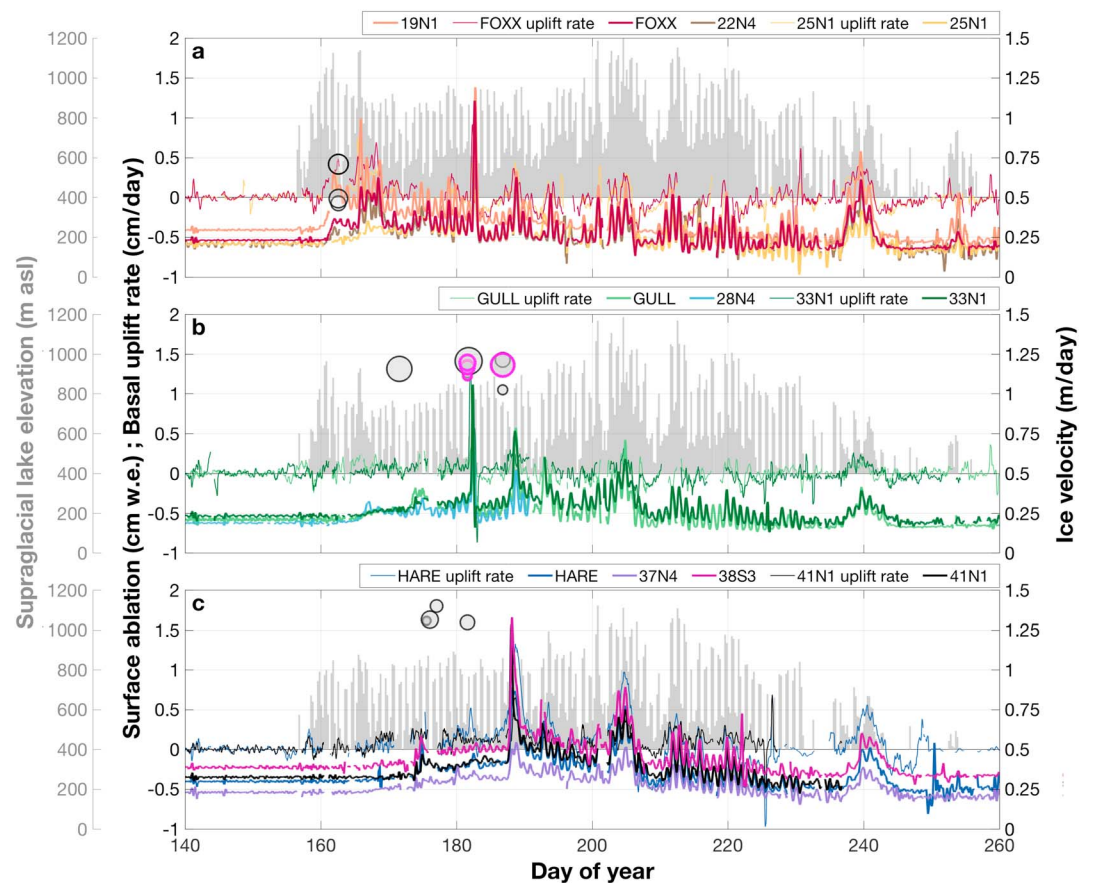


**Figure 3.** The 6-hr GPS-derived ice velocity (thick lines), basal uplift rates (thin lines), 6-hr modeled surface ablation (grey bars), and supraglacial lake drainages (grey circles) for 2011. Panels and descriptions are as in Figure 2.

(04:30 UTC), HARE (12:43 UTC), 33N1 (14:30 UTC), and GULL (17:45 UTC). These peak ice velocities all occurred before the typical timing of diurnal velocity peaks by at least 2 hr. At 37N4 and below GULL, peak velocities are indistinguishable from diurnal variations (Figure 3). Peak velocities suggest a lower propagation speed at moderate elevations. However, we note that the pattern and the location of the peak velocity, particularly HARE's and 38S3's extended period of elevated velocity (>24 hr), suggest slower and more complex water subglacial flow.

### 3.2. Longitudinal Strain Rates

Horizontal and vertical strain rates had similar magnitudes throughout the study area, though lateral (across-flow) strain rates had less variability over the observation period (Figure 4). Wintertime longitudinal strain rates were generally near zero or slightly compressional, except between 19N1 and FOXX (Figure 4). The onset of surface melting initiated a period of regional longitudinal extension and large positive strain rate anomalies, with the highest strain rates and strain rate anomalies occurring closest to the terminus (Figures 4a and 5a). Longitudinal strain rate anomalies remained positive until the supraglacial lake drainage event on day ~182. Following that lake drainage event, a period of relative regional compression occurred until day ~210, indicating that low-elevation locations had slowed relative to moderate-elevation locations (Figure 5a). Longitudinal strain rates recovered to wintertime values once daily minimum ice velocity dropped below winter background values. At that time (day ~210), a spatially alternating pattern of extension and compression emerged with extension generally dominating over ridges and compression dominating in basins (Figure 5a). Finally, the precipitation and melt event on day ~235 precipitated an increase in extension at low elevations, followed by increased compression at moderate elevations (Figure 5a).

The two observed lake-drainage events incited different strain rate patterns across the study area. During the first lake-drainage event, a focused wave of elevated compression, followed by elevated extension,

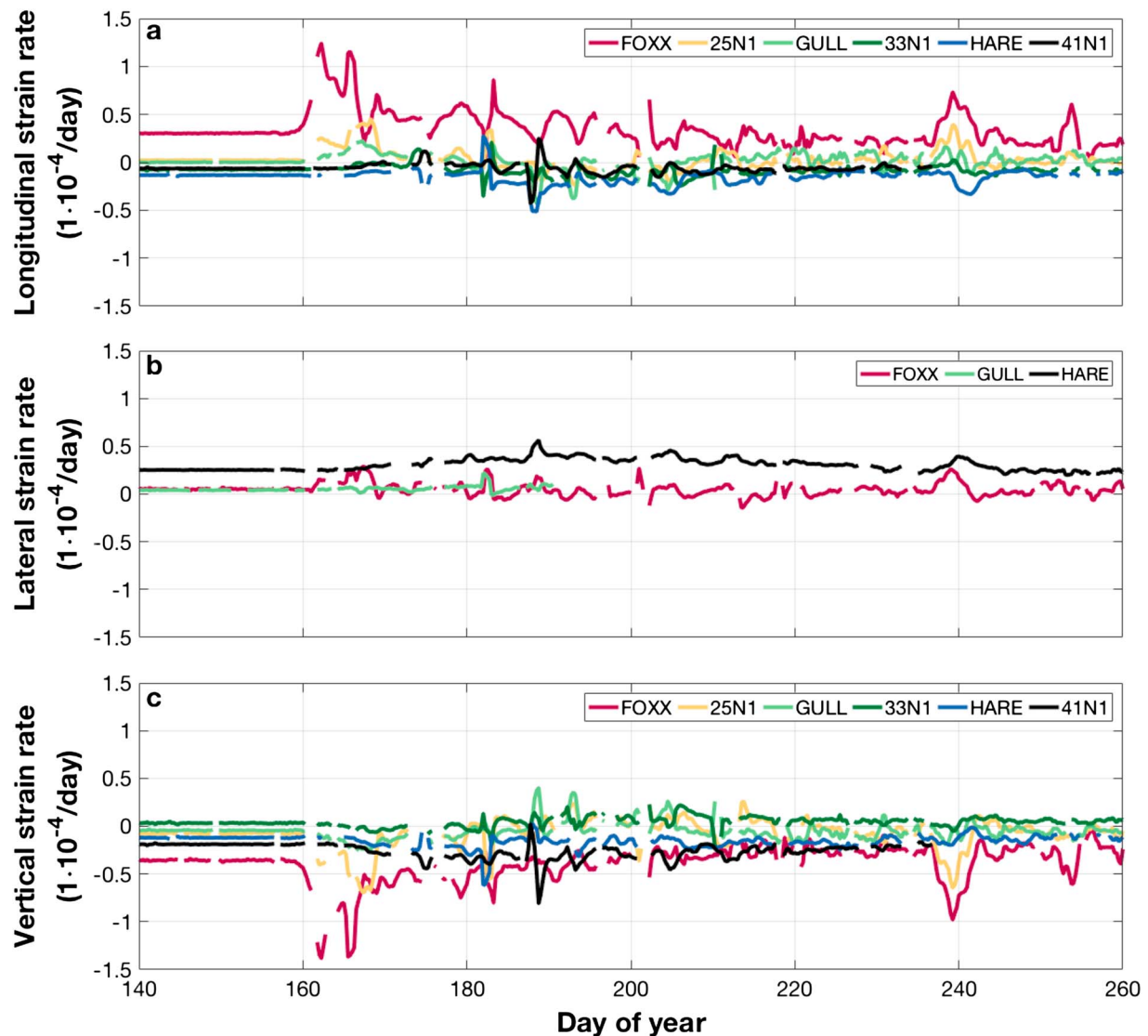


**Figure 4.** The 24-hr GPS-derived strain rates for the 2011 melt season, plotted every 4 hr for clarity. (a) Longitudinal strain rate calculated from stations along the flow line. (b) Lateral strain rate calculated from stations along and north of the central flow line. (c) Vertical strain rate calculated using continuity and assuming ice incompressibility.

propagated downstream (Figure 5b). This pattern may indicate the movement of former lake water through the subglacial hydrologic system. However, the second lake-drainage event (day ~188) triggered only an increase in compression, without any ensuing extension, potentially because the water could be readily accommodated by the subglacial system at lower elevations.

### 3.3. Basal Uplift

Maximum basal uplift ranged between 0.2 and 0.9 m (Figures 6a–6c). At FOXX, 25N1, and GULL, the timing of maximum basal uplift was closely associated with peak ice velocity and supraglacial lake drainage. However, at and above 33N1, peak ice velocity preceded maximum basal uplift by [Disregard empty mark up] 15 days, and at 41N1 (~1,050 m asl), we did not observe a decline in basal uplift (Figure 6c). Only basal uplift between FOXX and 25N1 returned to zero (or slightly negative) during the observation period, despite all horizontal ice velocities falling below their background speeds prior to the end of the melt season (Figure 6a). This behavior results in a correlation between ice velocity and basal uplift at elevations below 900 m asl ( $0.42 \leq r \leq 0.77$ ,  $p \leq 0.01$ ), but low or insignificant correlation at elevations above 900 m asl (Figures 7a–7c and Table 2).

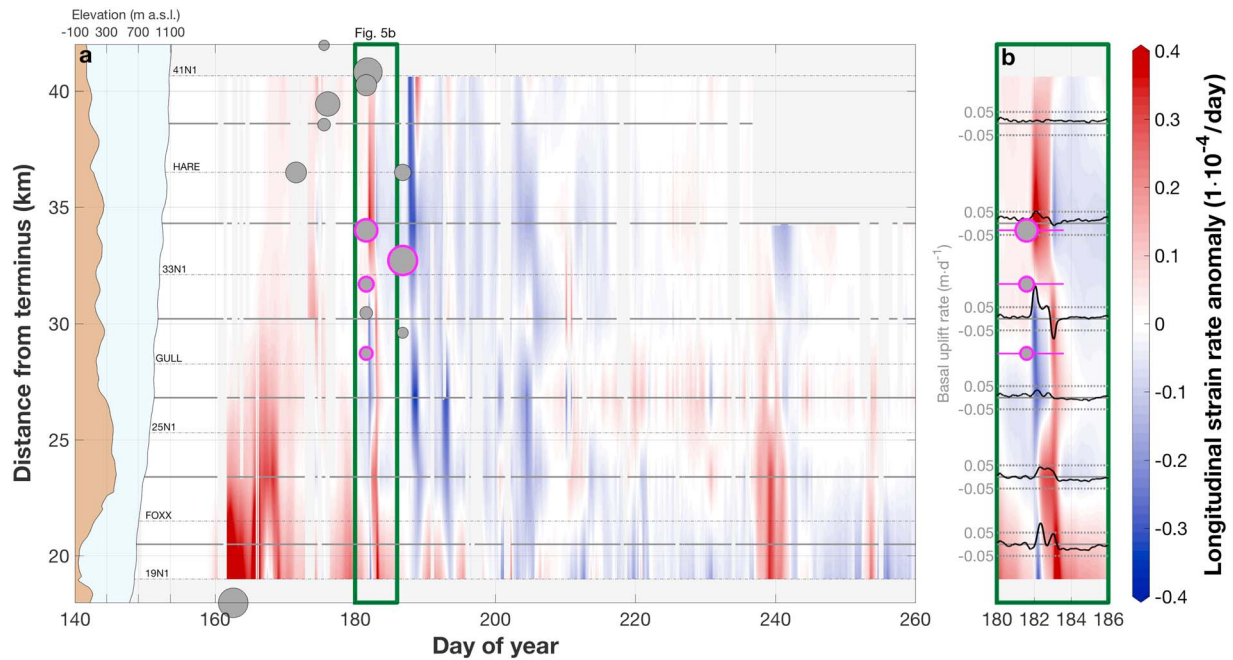


**Figure 5.** (a) Seasonal strain rate anomalies during the 2011 melt season. Anomalies are interpolated linearly between the midpoint between GPS stations (grey solid lines, broken sections indicate no data). GPS stations are plotted as distance from terminus (grey dashed lines). Values indicate the change in strain rate relative to the background magnitude (days 140–150). Negative values (blues) indicate regions of increased compression. Positive values (reds) indicate regions of extension. Supraglacial lake drainages (grey circles) are located by distance from terminus and scaled by maximum lake surface area (Morris et al., 2013). The pink outlines indicate lakes drainages that impacted observed ice velocities. Bed topography (brown shaded region) and ice thickness (blue shaded region) along the central flow line are indicated on the left side of panel (a). The green box indicates the time window displayed in (b). (b) Inset of strain rate anomalies and basal uplift rates (black lines) during the supraglacial lake cascade on day ~182. Lake drainages within the GPS network (grey circles, magenta outline) have a temporal uncertainty of  $\pm 2$  days (magenta bars; Morris et al., 2013).

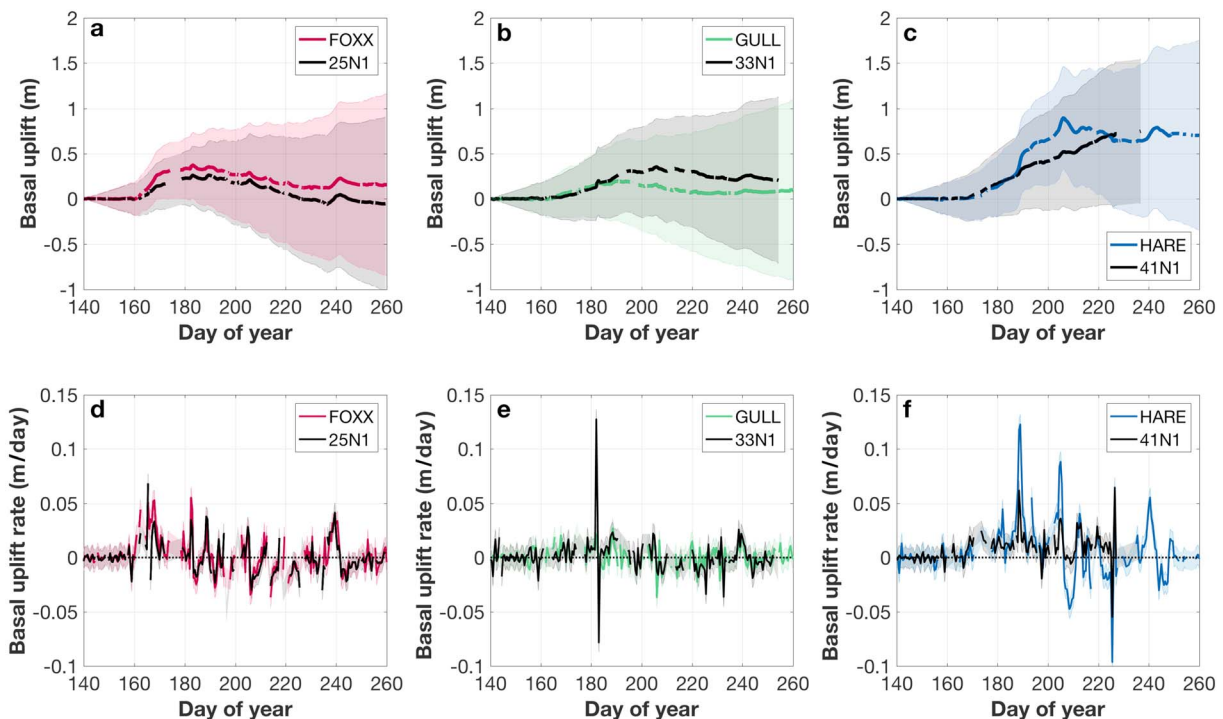


**Figure 6.** The (a–c) 24-hr basal uplift and (d–f) uplift rate of change by elevation grouping for 2011, plotted every 4 hr for clarity. Basal uplift and uplift rates are presented with uncertainties propagated from GPS-derived position.

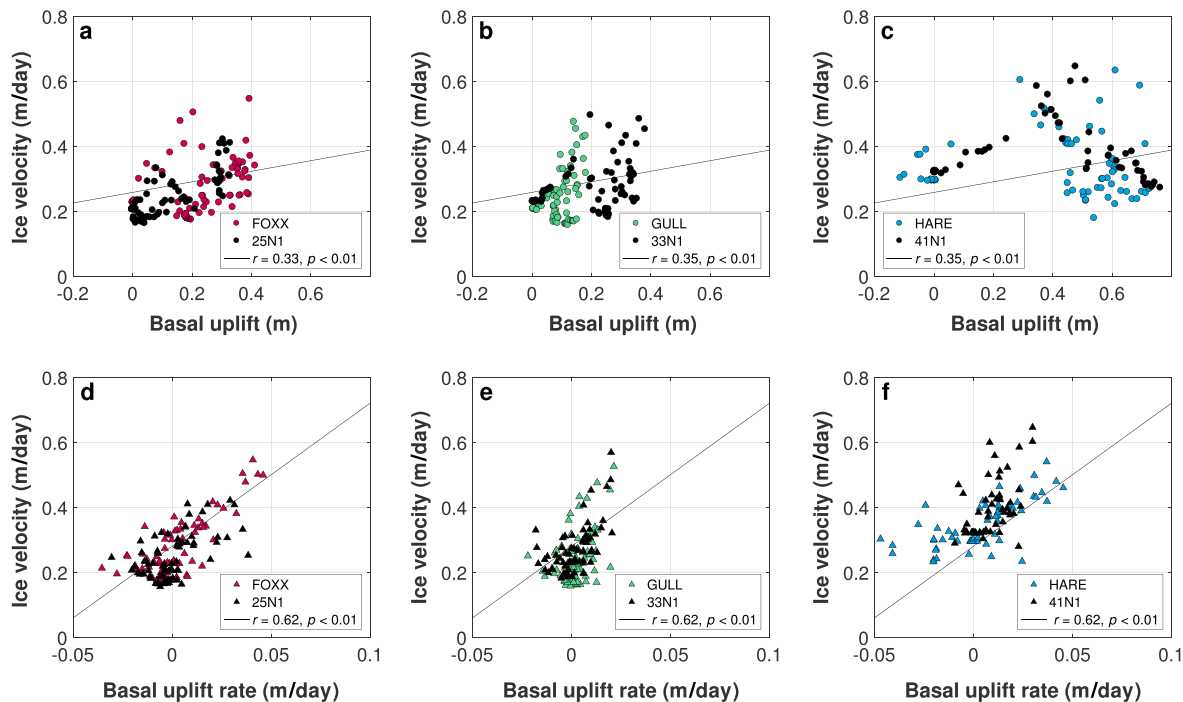


**Figure 7.** (a–c) Daily mean horizontal ice velocity as a function of daily mean basal uplift for each GPS location. (d–f) Daily mean horizontal ice velocity as a function of basal uplift rate for locations below 900 m asl and above 900 m asl locations. The linear best fit for each population (black line) and the associated correlation coefficient are indicated in the legend. Basal uplift rates during a supraglacial lake drainage at HARE are anomalously high and influence the calculated correlation between ice velocity and basal uplift rate. To remove this effect, we do not include basal uplift rates greater than 0.05 m/day in the determination of correlation coefficients.

During the early part of the melt season, we observed generally positive basal uplift rates, associated with rapidly increasing ice velocity (Figures 3 and 6d–6f). Maximum basal uplift rates were generally associated supraglacial lake drainage events, while strongly negative basal uplift rates occurred immediately following melt events or during periods of limited surface melt production. At FOXX, 25N1, and GULL, basal uplift rates became generally negative following lake drainage events, except during melt events. At 33N1 and HARE, basal uplift rates slow following lake drainage, but did not become frequently negative until day ~210; at 41N1, basal uplift rates tended to covary with surface melt, but remained generally positive for the observation period (Figures 3b and 3c). Overall, basal uplift rates and ice velocity tended to have stronger correlations across most locations ( $0.41 \leq r \leq 0.77$ ,  $p \leq 0.01$ ; Figure 7 and Table 2).

**Table 2**  
Correlation Coefficients for Each GPS Station

Location	$u \sim z_{bs}$	$u \sim \dot{c}$
FOXX	0.36	0.77
25N1	0.77	0.55
GULL	0.42	0.41
33N1	0.31	0.59
HARE	NS	0.69 <sup>a</sup>
41N1	NS	0.64
All locations	0.35	0.62

Note.  $u$  is horizontal ice velocity;  $z_{bs}$  is basal uplift;  $\dot{c}$  is basal uplift. All reported  $r$  have  $p$ -values less than 0.01. Basal uplift correlations at HARE and 41N1 were not significant (NS).

<sup>a</sup>Basal uplift rates at HARE during the day 188 supraglacial lake drainage are anomalously high and produce an artificially high correlation between ice velocity and basal uplift rate. To remove the influence of these outliers, we remove basal uplift rates greater than 0.05 m/day.

## 4. Discussion

### 4.1. Seasonal Evolution of Ice Motion

The staggered onset of summer ice acceleration at each site results in more than 20 days of strong extension at lower elevations, and negative vertical strain rates across the study area (Figures 4c and 5a). At low elevations, the subglacial hydrologic system was overwhelmed with available meltwater, resulting in an increase in subglacial pressure and ice velocity (Bartholomew et al., 2010; Hoffman et al., 2011). While at moderate elevations, where supraglacial meltwater production and drainage may be initially limited, ice acceleration was more gradual. This pattern generated a strain rate gradient roughly consistent with the inferred gradient in subglacial water supply (more tensile at the terminus, less tensile at moderate elevations; Figure 5a).

Prolonged snow cover at higher elevations causes the observed elevation gradient in seasonal ice-velocity response (e.g., Hoffman et al.,



2011; Hubbard & Nienow, 1997). But, in our study area, snow cover only remains extensive for approximately 10 days longer at HARE than at FOXX (until day ~168). Without snow cover, supraglacial meltwater retention on bare ice can become potentially important, particularly above ~900 m asl, where supraglacial lakes more prevalent (e.g., Koziol et al., 2017; Liang et al., 2012; Morriss et al., 2013). Retention of meltwater within supraglacial lakes can exacerbate spatial differences in meltwater delivery to the bed, resulting in a stronger gradient in ice acceleration and regionally tensile strain rate anomalies, which can trigger additional surface-to-bed connections, potentially including the observed lake drainages on day ~182 and ~188 in our study area (Figures 4a and 5a; Christoffersen et al., 2018; Hoffman et al., 2018).

Following the drainage of three supraglacial lakes on day ~182, the early season tensile strain rate anomaly terminated due to the onset of declining ice velocity and increased subglacial drainage efficiency below GULL (Hoffman et al., 2011; Sole et al., 2013; Sundal et al., 2011; Tedstone et al., 2013). This lake-drainage cascade was followed by a second cascade on day ~188 (Morriss et al., 2013), which is temporally associated with both the highest ice velocity and the initiation of long-term deceleration at stations from GULL to 41N1. Though the regional decline in ice velocity suggests a widespread subglacial response, an extended period of elevated compression across the region suggests that the efficiency of the subglacial system is spatially variable (day ~182–206, Figure 5a; Howat et al., 2008).

During this period, the cooccurrence of late-season ice deceleration and declining basal uplift at low elevations suggests that subglacial channelization is readily evacuating available meltwater at low pressure (Figures 3a and 6a; Bartholomew et al., 2010; Chandler et al., 2013). But, at locations above ~900 m asl ice decelerates more slowly, resulting in a compressional anomaly, and basal uplift rates are approximately zero (33N1) or remain generally positive (HARE and 41N1; Figures 6e and 6f). This disparity between declining ice velocity and increasing basal uplift suggests that—in these regions—subglacial channelization is slow and increasing subglacial drainage efficiency may be due to changes within the distributed system or changing pressures within the weakly connected system (Andrews et al., 2014; Bartholomew et al., 2011; Hoffman & Price, 2014; Hoffman et al., 2016; Iken & Truffer, 1997).

A melt event ending on day ~206 corresponds to the onset of basal uplift decline at 33N1 and HARE and the end of the regional compressional anomaly (Figures 2b and 2c and 5a). Following the melt event, strain rate anomalies at low elevations vacillate between elevated compression and extension, a pattern that persists through the end of the observation period. In our study area, ice at low elevations flows over a subglacial topography that alternates between overdeepening (19N1–FOXX), ridge (FOXX–25N1), and overdeepening (25N1–GULL; Figure 1c). The overdeepenings are likely at high pressure and filled with sediment, while above ridges the ice is more likely to be thinner and crevassed (Andrews et al., 2014; Ryser, Lüthi, Andrews, Catania, et al., 2014; Walter et al., 2014). Slightly lower subglacial drainage efficiency in the overdeepenings results in higher mean pressures and lower diurnal variability (Figure 3a; Dow et al., 2011; Hooke, 1991; Werder, 2016). Differences in diurnal variability can result in short-term variations in stress transfer and manifested as longitudinal strain rate perturbations (Figure 5a; Ryser, Lüthi, Andrews, Catania, et al., 2014). Our observations support the hypothesis that subglacial topography, in addition to hydrology, plays an important role in controlling local ice velocity, particularly in the late melt season (Fitzpatrick et al., 2013; Joughin et al., 2013; Palmer et al., 2011).

#### 4.2. Supraglacial Lake Drainage Impact on Ice Velocity

In our study area, supraglacial lake-drainage events induce maximum ice velocity and may trigger the transition between the ice sheet's early-season ice acceleration and late-season deceleration (Figures 2 and 3). The short-term impact of lake drainages on ice velocity is well documented, with ice speeds increasing substantially above background speeds during rapid supraglacial drainage events (Das et al., 2008; Hoffman et al., 2011; Stevens et al., 2015; Tedesco et al., 2013). However, their relative impact on the long-term evolution of the local and downstream subglacial hydrologic system and ice velocity is poorly understood, despite a number of field and remote-sensing observations that suggest supraglacial lake drainage may trigger the onset of late-season ice deceleration (Hoffman et al., 2011; Joughin et al., 2013; Sole et al., 2011).

The observed correlation between supraglacial lake drainage and ice deceleration may arise if the rapid flux of supraglacial lake water substantially modifies the subglacial hydrologic system and causes a significant increase in its drainage efficiency. At low elevations within our study area, water from lake drainage likely



enlarges small preexisting channels due to the excess of water and steeper hydraulic gradient associated with the lake drainages that occur on day ~182. This rapid growth could result in the subglacial system being able to readily accommodate subsequent meltwater and draw water from the surrounding distributed system, explaining both the observed gradual decline of ice velocity and the correlation between ice motion and basal uplift (Figures 2a and 7a and Table 2).

At moderate elevations in our study area, this hypothesis appears to be inconsistent with late-season ice deceleration that is generally associated with subglacial channelization because while ice velocity at these elevations begins to fall following the lake drainage event on day ~188, basal uplift continues to increase (Figures 2b–2c; Bartholomew et al., 2010; Chandler et al., 2013; Hoffman et al., 2011). However, supraglacial drainage events, like fast-rising jökulhlaups, are generally thought to occur so rapidly that subglacial channels cannot effectively develop in the vicinity of lake drainages and subglacial water flows as a turbulent sheet (Dow et al., 2015; Einarsson et al., 2017; Flowers et al., 2004; Werder & Funk, 2009). Increased subglacial efficiency, however, need not be confined to channelization alone (e.g., Andrews et al., 2014; Hoffman & Price, 2014; Meierbachtol et al., 2013). Instead, additional processes both at the surface and bed can alter the relationship between meltwater volume and local ice velocity.

The drainage of supraglacial lakes results in widespread strain rate perturbations (Figure 5b; Stevens et al., 2015), which can incite nearby lakes to drain in a cascade and open new surface-to-bed connections in the form of crevasses and moulins (Christoffersen et al., 2018; Hoffman et al., 2018). As in previous studies, in regions where supraglacial lakes are the dominant mechanism forming surface-to-bed connections, such cascades may flush a substantial fraction of the total volume of supraglacially stored water across a given region, causing ice acceleration followed by a reduced supraglacial water supply and regional ice deceleration (Clason et al., 2015; Joughin et al., 2013). This process may be particularly important at the highest locations in the study area, where diurnal variations remain muted until after the lake drainage event on day ~188 (Figures 2b and 2c). Despite potentially limited subglacial channel growth, the meltwater perturbation associated with supraglacial lake drainages may still substantially modify the bed conditions, possibly through expansion of the active part of the subglacial hydrologic system (Andrews et al., 2014; Hoffman et al., 2016), increased efficiency within the distributed system (Hoffman & Price, 2014; Meierbachtol et al., 2013), or sediment strengthening (Bougamont et al., 2014). Such increases in efficiency may explain why there is no significant correlation between observed ice velocity and basal uplift (unlike low elevation locations) but a reasonable correlation between ice velocity and basal uplift rate (Figure 7 and Table 2).

Several observational studies agree that supraglacial lake drainage may play a role in the seasonal transition of summer ice velocity from acceleration to deceleration. However, supraglacial lake drainages are not currently included in most models of the subglacial hydrologic system, in part due to the complexity of modeling ice-bed separation and turbulent sheet flow (e.g., Hewitt et al., 2012; Schoof et al., 2012). These models often cannot readily match observations of subglacial drainage efficiency in the natural system, as indicated by modeled ice velocity, potentially due a lack of two-way coupling between ice speed and subglacial hydrology (Hoffman & Price, 2014), lack of interannual subglacial memory, or poor constraints on subglacial characteristics (e.g., Gulley et al., 2014; Hewitt, 2013). However, our results suggest that the inability of subglacial models to adequately represent sudden and large water inputs is partly responsible for the current inability of these models to fully capture the observed evolution of the subglacial hydrologic system.

### 4.3. Subglacial Processes

At low elevation, ice velocity and basal uplift behave similarly over the course of the melt season and display a statistically significant positive correlation (Figures 2a and 2b and 7a and 7b and Table 2). This relationship is consistent with increasing subglacial drainage efficiency. There, the onset of the summer melt season is associated with the inability of the subglacial system to transmit the high supraglacial meltwater flux reaching the bed. The discrepancy results in increased subglacial water storage, leading to increased basal uplift, loss of basal traction, or elevated pore pressures in subglacial sediments, both of which can increase ice motion. As subglacial channelization expands, the lower pressure channels drain water stored in the distributed system, resulting in creep closure of subglacial cavities (Bartholomew et al., 2008; Bartholomew et al., 2010; Harper et al., 2007; Howat et al., 2008; Iken et al., 1983; Kamb et al., 1994) or reduced sediment pore pressure (Walter et al., 2014), both of which reduce ice motion and result in a decline in basal uplift. Therefore, ice velocity is positively associated with both the magnitude of basal uplift and its rate of change (Table 2; Howat

et al., 2008; Iken, 1981). However, above ~900 m asl, we observe periods when ice velocity declines as basal uplift continues to increase (Figures 2b and 2c, days 188–206 for 33N1 and HARE and days 188–227 for 41N1), complicating any seasonal relationship between these two observations (Table 2 and Figure 7). Similar behavior was observed in 2007 by Hoffman et al. (2011), with increasing basal uplift corresponding with decreasing ice motion at several locations (their GPS stations 307, 407, 507, and Wild1) within and slightly above our study area.

The increasingly poor relationship between ice velocity and basal uplift at progressively higher elevations appears to require an explanation beyond the development of extensive subglacial channelization. However, the poorly constrained state of the bed makes it difficult to determine the exact mechanism of increasing subglacial efficiency. We hypothesize that, where channel development is limited (Banwell et al., 2016) and subglacial pressure is generally at or above overburden pressure (Wright et al., 2016), the observed decline in ice velocity during periods of increasing basal uplift is likely due to changing efficiency within subglacial cavities (Andrews et al., 2014; Hoffman et al., 2016; Iken & Truffer, 1997; Meierbachtol et al., 2013), extensive sediment dilation (Clarke, 2005), or some combination of these processes.

Under hard-bedded conditions, cavity growth rates act as a primary control on ice velocity. The highest velocities are associated with cavity expansion, due to a significant component forward displacement caused by cavity growth; lower velocities are associated with cavity closure, because creep closure acts primarily in the vertical direction, resulting in a positive relationship between the daily basal uplift rate and ice velocity for the duration of the melt season (Figures 7c–7f and Table 2; Cowton et al., 2016; Iken, 1981). Generally, cavity growth and forward motion is associated with increased subglacial water storage and higher water pressure (e.g., Bartholomäus et al., 2008; Kamb et al., 1994; Sugiyama & Gudmundsson, 2004). However, basal sliding can also act to open and connect subglacial cavities, even in the absence of extensive subglacial channelization (Bartholomäus et al., 2011; Hoffman & Price, 2014), increasing their ability to transport meltwater (Iken & Truffer, 1997; Meierbachtol et al., 2013), reducing subglacial water pressure and confounding any correlation between basal uplift and ice motion as observed at 33N1, HARE, and 41N1 during part of the melt season (Figures 2b and 2c and 7b and 7c; Harper et al., 2005, 2007). Additionally, above 900 m asl, where moulins are relatively sparse, extensive regions of the bed may be weakly connected or unconnected to the hydrologically active part of the bed (Andrews et al., 2014; Iken et al., 1983). In these regions, increased subglacial pressure and sliding in active regions of the bed can be mitigated when this sliding causes cavity growth in isolated or weakly-connected regions of the bed, resulting in widespread reductions in pressure (Andrews et al., 2014; Hoffman et al., 2016; Iken & Truffer, 1997).

Alternatively, limitations in the development of efficient subglacial channels can result in sediments remaining relatively undrained. Under these conditions, sediment strengthening and reduction in pore pressure can act to inhibit sediment deformation when the sediment's critical-state porosity is not attained (Clarke, 1987; Iverson et al., 1998), potentially causing ice deceleration despite increased basal uplift (Figures 2b and 2c). If, during the course of the melt season, subglacial channels or canals grow enough to readily conduct the available water, dewatering can occur, resulting in sediment compaction and stiffening (Walter et al., 2014). This may be the cause of the return of a correlated relationship between ice velocity and basal uplift at 33N1 and HARE during that late melt season (Figures 2b and 2c). However, this relationship may be complicated by the potentially patchy nature of sediments in some regions, which may be the reason that daily ice velocity and uplift rates remain positively correlated, even at high elevations (Figure 7d and Table 2; Hoffman et al., 2016; Ryser, Lüthi, Andrews, Catania, et al., 2014). The transfer of mechanical support from regions with either high subglacial sediment conductivity or hard-bedded conditions during daily periods of high melt input to these regions can induce diurnal variations in ice motion, which correlate to basal uplift rates (Meierbachtol et al., 2016; Murray & Clarke, 1995; Truffer et al., 2001).

Against the backdrop of a seasonally and interannually evolving subglacial hydrologic system, these complex interrelationships explain why the correlation between ice velocity and basal uplift varies spatially (Figures 2 and 7 and Table 2) and emphasizes the need for further characterization of subglacial conditions. Though modern sliding laws are constructed on the aforementioned relationship between regional subglacial pressure and ice motion (e.g., Gagliardini et al., 2007; Schoof, 2005), basal sliding can depend on both subglacial water pressure and the size of basal cavities (Iken, 1981). The extent of cavitation affects the distribution of bed normal stress, such that larger normal stress gradients associated with larger subglacial cavities will

result in a decrease in basal sliding for the same water pressure (Howat et al., 2008; Iken, 1981). Further, the presence of extensive subglacial sediments (e.g., Dow et al., 2013; Walter et al., 2014) can result in subglacial water pressure being dependent on time- and space-varying sediment properties (Boulton et al., 1974; Clarke, 1987).

## 5. Conclusions

Beyond ice velocity, data derived from GPS positions can provide substantial insight into the state of the subglacial hydrologic system. Our observations suggest that the timing of the transition from primarily inefficient to efficient subglacial drainage may be accelerated by supraglacial lake drainages. The complex relationship between ice velocity and basal uplift suggests that above 900 m asl, where subglacial channelization may be limited, changing connectivity within inefficient subglacial drainage elements or the presence of subglacial sediments could explain periods when the ice sheet decelerates despite continuing basal uplift. Thus, explicit and improved representation of rapid subglacial water fluxes from supraglacial lake drainages and improved basal friction relationships are likely necessary to accurately model seasonal subglacial and ice dynamic behavior as surface melt increases at higher elevations.

## Author Contributions

L. C. A. analyzed and interpreted the data and wrote the manuscript. M. J. H. aided with data processing and interpretation. G. A. C., T. A. N., M. P. L., and R. L. H. designed the original study. M. J. H., L. C. A., T. A. N., M. P. L., R. L. H., K. M. S., C. R., and B. F. M. all contributed substantially to fieldwork. All authors discussed the results and provided feedback.

## Acknowledgments

This project was supported by U.S. National Science Foundation grants OPP-0908156, OPP-0909454, and ANT-0424589 (to CREIS) and Swiss National Science Foundation grant 200021\_127197. Support for L. C. A. was provided by an appointment to the NASA Postdoctoral Program at the Goddard Space Flight Center, administered by Universities Space Research Association under contract with NASA and by the Global Modeling and Assimilation Office at NASA Goddard Space Flight Center funded under the NASA Modeling, Analysis, and Prediction (MAP) Program. M. J. H. was supported by NASA Cryospheric Sciences and Climate Modeling Programs within the U.S. Department of Energy, Office of Science. Logistical support was provided by CH2MHill Polar Services. The GPS base station and several on-ice GPS units were provided by the UNAVCO facility with support from the NSF and NASA under cooperative agreement EAR-0735156. We thank Kristin Poinar and Joseph MacGregor for feedback on drafts of this manuscript. We also thank Editor, Bryn Hubbard, and three anonymous reviewers their thoughtful and constructive comments. The data presented within this manuscript are accessible by download via the NSF Arctic Data Center (<https://arcticdata.io;doi.org/10.18739/A2F504>).

## References

- Anderson, R. S., Anderson, S. P., MacGregor, K. R., Waddington, E. D., O'Neel, S., Riihimäki, C. A., & Loso, M. G. (2004). Strong feedbacks between hydrology and sliding of a small alpine glacier. *Journal of Geophysical Research*, 109, F03005. <https://doi.org/10.1029/2004JF000120>
- Andrews, L. C. (2015). Spatial and temporal evolution of the glacial hydrologic system of the Western Greenland Ice Sheet: Observational and remote sensing results (PhD). The University of Texas at Austin, Austin, TX.
- Andrews, L. C., Catania, G. A., Hoffman, M. J., Gulle, J. D., Lüthi, M. P., Ryser, C., et al. (2014). Direct observations of evolving subglacial drainage beneath the Greenland Ice Sheet. *Nature*, 514(7520), 80–83. <https://doi.org/10.1038/nature13796>
- Banwell, A. F., Hewitt, I., Willis, I., & Arnold, N. (2016). Moulin density controls drainage development beneath the Greenland ice sheet. *Journal of Geophysical Research: Earth Surface*, 121, 2248–2269. <https://doi.org/10.1002/2015JF003801>
- Bartholomäus, T. C., Anderson, R. S., & Anderson, S. P. (2008). Response of glacier basal motion to transient water storage. *Nature Geoscience*, 1(1), 33–37. <https://doi.org/10.1038/ngeo.2007.52>
- Bartholomäus, T. C., Anderson, R. S., & Anderson, S. P. (2011). Growth and collapse of the distributed subglacial hydrologic system of Kennicott Glacier, Alaska, USA, and its effects on basal motion. *Journal of Glaciology*, 57(206), 985–1002. <https://doi.org/10.3189/002214311798843269>
- Bartholomew, I. D., Nienow, P., Mair, D., Hubbard, A., King, M. A., & Sole, A. (2010). Seasonal evolution of subglacial drainage and acceleration in a Greenland outlet glacier. *Nature Geoscience*, 3(6), 408–411. <https://doi.org/10.1038/ngeo863>
- Bartholomew, I. D., Nienow, P., Sole, A., Mair, D., Cowton, T., King, M. A., & Palmer, S. (2011). Seasonal variations in Greenland Ice Sheet motion: Inland extent and behaviour at higher elevations. *Earth and Planetary Science Letters*, 307(3–4), 271–278. <https://doi.org/10.1016/j.epsl.2011.04.014>
- Bougamon, M., Christoffersen, P., Hubbard, A. L., Fitzpatrick, A. A., Doyle, S. H., & Carter, S. P. (2014). Sensitive response of the Greenland Ice Sheet to surface melt drainage over a soft bed. *Nature Communications*, 5(1). <https://doi.org/10.1038/ncomms6052>
- Boulton, G. S., Dent, D. L., & Morris, E. M. (1974). Subglacial shearing and crushing, and the role of water pressures in tills from South-East Iceland. *Geografiska Annaler. Series A, Physical Geography*, 56(3–4), 135–145. <https://doi.org/10.1080/04353676.1974.11879895>
- Box, J. E., Fettweis, X., Stroeve, J. C., Tedesco, M., Hall, D. K., & Steffen, K. (2012). Greenland ice sheet albedo feedback: Thermodynamics and atmospheric drivers. *The Cryosphere*, 6(4), 821–839. <https://doi.org/10.5194/tc-6-821-2012>
- Chandler, D. M., Wadham, J. L., Lis, G. P., Cowton, T., Sole, A., Bartholomew, I., et al. (2013). Evolution of the subglacial drainage system beneath the Greenland Ice Sheet revealed by tracers. *Nature Geoscience*, 6(3), 195–198. <https://doi.org/10.1038/ngeo1737>
- Chen, G. (1998). *GPS kinematic positioning for airborne laser altimetry at Long Valley, California*. Cambridge, MA: Massachusetts Institute of Technology. Retrieved from <http://dspace.mit.edu/handle/1721.1/9680>
- Christoffersen, P., Bougamon, M., Hubbard, A., Doyle, S. H., Grigsby, S., & Pettersson, R. (2018). Cascading lake drainage on the Greenland Ice Sheet triggered by tensile shock and fracture. *Nature Communications*, 9(1), 1064. <https://doi.org/10.1038/s41467-018-03420-8>
- Clarke, G. K. C. (1987). Subglacial till: A physical framework for its properties and processes. *Journal of Geophysical Research*, 92, 9023–9036. <https://doi.org/10.1029/JB092iB09p09023>
- Clarke, G. K. C. (2005). Subglacial Processes. *Annual Review of Earth and Planetary Sciences*, 33(1), 247–276. <https://doi.org/10.1146/annurev.earth.33.092203.122621>
- Clason, C. C., Mair, D. W. F., Nienow, P. W., Bartholomew, I. D., Sole, A., Palmer, S., & Schwanghart, W. (2015). Modelling the transfer of supraglacial meltwater to the bed of Leverett Glacier, Southwest Greenland. *The Cryosphere*, 9(1), 123–138. <https://doi.org/10.5194/tc-9-123-2015>
- Cowton, T., Nienow, P., Bartholomew, I., & Mair, D. (2016). Variability in Ice Motion at a Land-Terminating Greenlandic Outlet Glacier: The Role of Channelized and Distributed Drainage Systems. *Journal of Glaciology*, 62, 451–466. <https://doi.org/10.1017/jog.2016.36>

- Das, S. B., Joughin, I., Behn, M. D., Howat, I. M., King, M. A., Lizarralde, D., & Bhatia, M. P. (2008). Fracture propagation to the base of the Greenland Ice Sheet during supraglacial lake drainage. *Science*, 320(5877), 778–781. <https://doi.org/10.1126/science.1153360>
- Dow, C. F., Hubbard, A., Booth, A. D., Doyle, S. H., Gusmeroli, A., & Kulesa, Y. B. (2013). Seismic evidence of mechanically weak sediments underlying Russell Glacier, West Greenland. *Annals of Glaciology*, 54(64), 135–141. <https://doi.org/10.3189/2013AoG64A032>
- Dow, C. F., Kavanaugh, J. L., Sanders, J. W., Cuffey, K. M., & MacGregor, K. R. (2011). Subsurface hydrology of an overdeepened cirque glacier. *Journal of Glaciology*, 57(206), 1067–1078. <https://doi.org/10.3189/002214311798843412>
- Dow, C. F., Kulesa, B., Rutt, I. C., Tsai, V. C., Pimentel, S., Doyle, S. H., et al. (2015). Modeling of subglacial hydrological development following rapid supraglacial lake drainage. *Journal of Geophysical Research: Earth Surface*, 120, 1127–1147. <https://doi.org/10.1002/2014JF003333>
- Doyle, S. H., Hubbard, A., Fitzpatrick, A. A. W., van As, D., Mikkelsen, A. B., Pettersson, R., & Hubbard, B. (2014). Persistent flow acceleration within the interior of the Greenland ice sheet. *Geophysical Research Letters*, 41, 899–905. <https://doi.org/10.1002/2013GL058933>
- Doyle, S. H., Hubbard, A., van de Wal, R. S. W., Box, J. E., van As, D., Scharrer, K., et al. (2015). Amplified melt and flow of the Greenland ice sheet driven by late-summer cyclonic rainfall. *Nature Geoscience*, 8(8), 647–653. <https://doi.org/10.1038/ngeo2482>
- Einarsson, B., Jóhannesson, T., Thorsteinsson, T., Gaidos, E., & Zwinger, T. (2017). Subglacial flood path development during a rapidly rising jökulhlaup from the western Skaftá cauldron, Vatnajökull, Iceland. *Journal of Glaciology*, 63, 670–682. <https://doi.org/10.1017/jog.2017.33>
- Fitzpatrick, A. A. W., Hubbard, A. L., Box, J. E., Quincey, D. J., van As, D., Mikkelsen, A. P. B., et al. (2014). A decade (2002–2012) of supraglacial lake volume estimates across Russell Glacier, West Greenland. *The Cryosphere*, 8(1), 107–121. <https://doi.org/10.5194/tc-8-107-2014>
- Fitzpatrick, A. A. W., Hubbard, A., Joughin, I., Quincey, D. J., van As, D., Mikkelsen, A. P. B., et al. (2013). Ice flow dynamics and surface meltwater flux at a land-terminating sector of the Greenland ice sheet. *Journal of Glaciology*, 59(216), 687–696. <https://doi.org/10.3189/2013JoG12J143>
- Flowers, G. E., Björnsson, H., Pálsson, F., & Clarke, G. K. C. (2004). A coupled sheet-conduit mechanism for jökulhlaup propagation. *Geophysical Research Letters*, 31, L05401. <https://doi.org/10.1029/2003GL019088>
- Gagliardini, O., Cohen, D., Råback, P., & Zwinger, T. (2007). Finite-element modeling of subglacial cavities and related friction law. *Journal of Geophysical Research*, 112, F02027. <https://doi.org/10.1029/2006JF000576>
- Gulley, J. D., Spellman, P. D., Covington, M. D., Martin, J. B., Benn, D. I., & Catania, G. (2014). Large values of hydraulic roughness in subglacial conduits during conduit enlargement: Implications for modeling conduit evolution. *Earth Surface Processes and Landforms*, 39(3), 296–310. <https://doi.org/10.1002/esp.3447>
- Hall, D. K., Salomonson, V. V., & Riggs, G. A. (2006). MODIS/Terra snow cover daily L3 global 500 m grid. Version 5. [May 2011–September 2012]. Boulder, Colorado: NASA National Snow and Ice Data Distributed Active Archive Center. Retrieved from <https://doi.org/10.5067/63NQRSRDPDB0>
- Harper, J. T., Humphrey, N. F., Pfeffer, W. T., Fudge, T., & O'Neel, S. (2005). Evolution of subglacial water pressure along a glacier's length. *Annals of Glaciology*, 40(1), 31–36. <https://doi.org/10.3189/172756405781813573>
- Harper, J. T., Humphrey, N. F., Pfeffer, W. T., & Lazar, B. (2007). Two modes of accelerated glacier sliding related to water. *Geophysical Research Letters*, 34, L12503. <https://doi.org/10.1029/2007GL030233>
- Hewitt, I. J. (2013). Seasonal changes in ice sheet motion due to melt water lubrication. *Earth and Planetary Science Letters*, 371–372, 16–25. <https://doi.org/10.1016/j.epsl.2013.04.022>
- Hewitt, I. J., Schoof, C., & Werder, M. A. (2012). Flotation and free surface flow in a model for subglacial drainage. Part 2. Channel flow. *Journal of Fluid Mechanics*, 702, 157–187. <https://doi.org/10.1017/jfm.2012.166>
- Hoffman, M. J., Andrews, L. C., Price, S. A., Catania, G. A., Neumann, T. A., Lüthi, M. P., et al. (2016). Greenland subglacial drainage evolution regulated by weakly connected regions of the bed. *Nature Communications*, 7, 13903. <https://doi.org/10.1038/ncomms13903>
- Hoffman, M. J., Catania, G. A., Neumann, T. A., Andrews, L. C., & Rummel, J. A. (2011). Links between acceleration, melting, and supraglacial lake drainage of the western Greenland ice sheet. *Journal of Geophysical Research*, 116, F04035. <https://doi.org/10.1029/2010JF001934>
- Hoffman, M. J., Perego, M., Andrews, L. C., Price, S. F., Neumann, T. A., Johnson, J. V., et al. (2018). Widespread moulin formation during supraglacial Lake drainages in Greenland. *Geophysical Research Letters*, 45, 778–788. <https://doi.org/10.1002/2017GL075659>
- Hoffman, M. J., & Price, S. (2014). Feedbacks between coupled subglacial hydrology and glacier dynamics. *Journal of Geophysical Research: Earth Surface*, 119, 414–436. <https://doi.org/10.1002/2013JF002943>
- Hooke, R. L. (1991). Positive feedbacks associated with erosion of glacial cirques and overdeepenings. *GSA Bulletin*, 103(8), 1104–1108. [https://doi.org/10.1130/0016-7606\(1991\)103<1104:PFAWEO>2.3.CO;2](https://doi.org/10.1130/0016-7606(1991)103<1104:PFAWEO>2.3.CO;2)
- Howat, I. M., Negrete, A., & Smith, B. E. (2014). The Greenland Ice Mapping Project (GIMP) land classification and surface elevation data sets. *The Cryosphere*, 8(4), 1509–1518. <https://doi.org/10.5194/tc-8-1509-2014>
- Howat, I. M., Negrete, A., & Smith, B. E. (2015). MEaSUREs Greenland Ice Mapping Project (GIMP) digital elevation model, Version 1. Boulder, Colorado: NASA National Snow and Ice Data Distributed Active Archive Center. [Retrieved from <https://doi.org/10.5067/NV34YUJXLP9WJ>]
- Howat, I. M., Tulaczyk, S., Waddington, E., & Björnsson, H. (2008). Dynamic controls on glacier basal motion inferred from surface ice motion. *Journal of Geophysical Research*, 113, F03015. <https://doi.org/10.1029/2007JF000925>
- Hubbard, B. P., & Nienow, P. (1997). Alpine subglacial hydrology. *Quaternary Science Reviews*, 16(9), 939–955. [https://doi.org/10.1016/S0277-3791\(97\)00031-0](https://doi.org/10.1016/S0277-3791(97)00031-0)
- Ignéczi, Á., Sole, A. J., Livingstone, S. J., Leeson, A., Fettweis, X., Selmes, N., et al. (2016). North-east sector of the Greenland Ice Sheet to undergo the greatest inland expansion of supraglacial lakes during the 21st century. *Geophysical Research Letters*, 43, 9729–9738. <https://doi.org/10.1002/2016GL070338>
- Iken, A. (1981). The effect of the subglacial water pressure on the sliding velocity of a glacier in an idealized numerical model. *Journal of Glaciology*, 27(97), 407–421. <https://doi.org/10.3189/1981JoG27-97-407-421>
- Iken, A., & Bindshadler, R. (1986). Combined measurements of subglacial water pressure and surface velocity of Findelengletscher, Switzerland: Conclusions about drainage system and sliding mechanism. *Journal of Glaciology*, 32(110), 101–119. <https://doi.org/10.3189/S0022143000006936>
- Iken, A., Röthlisberger, H., Flotron, A., & Haeblerli, W. (1983). The uplift of Unteraargletscher at the beginning of the melt season—A consequence of water storage at the bed? *Journal of Glaciology*, 29(101), 28–47. <https://doi.org/10.3189/S0022143000005128>
- Iken, A., & Truffer, M. (1997). The relationship between subglacial water pressure and velocity of Findelengletscher, Switzerland, during its advance and retreat. *Journal of Glaciology*, 43(144), 328–338. <https://doi.org/10.3189/S0022143000003282>
- Iverson, N. R., Hooyer, T. S., & Baker, R. W. (1998). Ring-shear studies of till deformation: Coulomb-plastic behavior and distributed strain in glacier beds. *Journal of Glaciology*, 44(148), 634–642. <https://doi.org/10.3189/S0022143000002136>
- Joughin, I., Das, S. B., Flowers, G. E., Behn, M. D., Alley, R. B., King, M. A., et al. (2013). Influence of ice-sheet geometry and supraglacial lakes on seasonal ice-flow variability. *The Cryosphere*, 7(4), 1185–1192. <https://doi.org/10.5194/tc-7-1185-2013>



- Joughin, I., Smith, B., Howat, I., & Scambos, T. (2016). MEASURES multi-year Greenland ice sheet velocity mosaic, version 1. Boulder, Colorado: NASA National Snow and Ice Data Distributed Active Archive Center. <https://doi.org/10.5067/QUASQ95VMSJG>
- Joughin, I., Smith, B. E., Howat, I. M., Scambos, T., & Moon, T. (2010). Greenland flow variability from ice-sheet-wide velocity mapping. *Journal of Glaciology*, 56(197), 415–430. <https://doi.org/10.3189/002214310792447734>
- Kamb, B., Engelhardt, H., Fahnestock, M. A., Humphrey, N., Meier, M., & Stone, D. (1994). Mechanical and hydrologic basis for the rapid motion of a large tidewater glacier: 2. Interpretation. *Journal of Geophysical Research*, 99, 15,231–15,244. <https://doi.org/10.1029/94JB00467>
- Kozioł, C., Arnold, N., Pope, A., & Colgan, W. (2017). Quantifying supraglacial meltwater pathways in the Paakitsoq region, West Greenland. *Journal of Glaciology*, 63, 464–476. <https://doi.org/10.1017/jog.2017.5>
- Leeson, A. A., Shepherd, A., Briggs, K., Howat, I., Fettweis, X., Morlighem, M., & Rignot, E. (2015). Supraglacial lakes on the Greenland ice sheet advance inland under warming climate. *Nature Climate Change*, 5(1), 51–55. <https://doi.org/10.1038/nclimate2463>
- Liang, Y.-L., Colgan, W., Lv, Q., Steffen, K., Abdalati, W., Stroeve, J., et al. (2012). A decadal investigation of supraglacial lakes in West Greenland using a fully automatic detection and tracking algorithm. *Remote Sensing of Environment*, 123, 127–138. <https://doi.org/10.1016/j.rse.2012.03.020>
- Mair, D., Sharp, M. J., & Willis, I. C. (2002). Evidence for basal cavity opening from analysis of surface uplift during a high-velocity event: Haut Glacier d'Arolla, Switzerland. *Journal of Glaciology*, 48(161), 208–216. <https://doi.org/10.3189/172756502781831502>
- Meierbachtol, T. W., Harper, J., & Humphrey, N. (2013). Basal drainage system response to increasing surface melt on the Greenland Ice Sheet. *Science*, 341(6147), 777–779. <https://doi.org/10.1126/science.1235905>
- Meierbachtol, T. W., Harper, J. T., Humphrey, N. F., & Wright, P. J. (2016). Mechanical forcing of water pressure in a hydraulically isolated reach beneath western Greenland's ablation zone. *Annals of Glaciology*, 57(72), 1–9. <https://doi.org/10.1017/aog.2016.5>
- Morlighem, M., Rignot, E., Mouginot, J., Seroussi, H., & Larour, E. (2014). Deeply incised submarine glacial valleys beneath the Greenland ice sheet. *Nature Geoscience*, 7(6), 418–422. <https://doi.org/10.1038/ngeo2167>
- Morlighem, M., Rignot, E., Mouginot, J., Seroussi, H., & Larour, E. (2015). IceBridge BedMachine Greenland, version 2. Boulder, Colorado: NASA National Snow and Ice Data Distributed Active Archive Center. <https://doi.org/10.5067/AD7B0HQNSJ29>
- Morriss, B. F., Hawley, R. L., Chipman, J. W., Andrews, L. C., Catania, G. A., Hoffman, M. J., et al. (2013). A ten-year record of supraglacial lake evolution and rapid drainage in West Greenland using an automated processing algorithm for multispectral imagery. *The Cryosphere*, 7(6), 1869–1877. <https://doi.org/10.5194/tc-7-1869-2013>
- Murray, T., & Clarke, G. K. C. (1995). Black-box modeling of the subglacial water system. *Journal of Geophysical Research*, 100, 10,231–10,245. <https://doi.org/10.1029/95JB00671>
- Nienow, P. W., Sole, A. J., Slater, D. A., & Cowton, T. R. (2017). Recent advances in our understanding of the role of meltwater in the Greenland Ice Sheet System. *Current Climate Change Reports*, 3(4), 330–344. <https://doi.org/10.1007/s40641-017-0083-9>
- Nienow, P. W., Sharp, M. J., & Willis, I. (1998). Seasonal change in the morphology of the subglacial drainage system, Haut Glacier D'Arolla, Switzerland. *Earth Surface Processes and Landforms*, 23, 825–843. [https://doi.org/10.1002/\(SICI\)1096-9837\(199809\)23:9%3C825::AID-ESP893%3E3.0.CO;2%E2%80%93932](https://doi.org/10.1002/(SICI)1096-9837(199809)23:9%3C825::AID-ESP893%3E3.0.CO;2%E2%80%93932)
- Palmer, S., Shepherd, A., Nienow, P., & Joughin, I. (2011). Seasonal speedup of the Greenland Ice Sheet linked to routing of surface water. *Earth and Planetary Science Letters*, 302(3–4), 423–428. <https://doi.org/10.1016/j.epsl.2010.12.037>
- Pellicciotti, F., Brock, B., Strasser, U., Burlando, P., Funk, M., & Corripio, J. (2005). An enhanced temperature-index glacier melt model including the shortwave radiation balance: Development and testing for Haut Glacier d'Arolla, Switzerland. *Journal of Glaciology*, 51(175), 573–587. <https://doi.org/10.3189/172756505781829124>
- Price, S. F., Payne, A. J., Catania, G. A., & Neumann, T. A. (2008). Seasonal acceleration of inland ice via longitudinal coupling to marginal ice. *Journal of Glaciology*, 54(185), 213–219. <https://doi.org/10.3189/002214308784886117>
- Ryser, C., Lüthi, M. P., Andrews, L. C., Catania, G. A., Funk, M., Hawley, R. L., et al. (2014). Caterpillar-like ice motion in the ablation zone of the Greenland ice sheet. *Journal of Geophysical Research: Earth Surface*, 119, 2258–2271. <https://doi.org/10.1002/2013JF003067>
- Ryser, C., Lüthi, M. P., Andrews, L. C., Hoffman, M. J., Catania, G. A., Hawley, R. L., et al. (2014). Sustained high basal motion of the Greenland ice sheet revealed by borehole deformation. *Journal of Glaciology*, 60(222), 647–660. <https://doi.org/10.3189/2014JG13J196>
- Schoof, C. (2005). The effect of cavitation on glacier sliding. *Proceedings of the Royal Society A: Mathematical, Physical and Engineering Sciences*, 461(2055), 609–627. <https://doi.org/10.1098/rspa.2004.1350>
- Schoof, C. (2010). Ice-sheet acceleration driven by melt supply variability. *Nature*, 468(7325), 803–806. <https://doi.org/10.1038/nature09618>
- Schoof, C., Hewitt, I. J., & Werder, M. A. (2012). Flotation and free surface flow in a model for subglacial drainage. Part 1. Distributed drainage. *Journal of Fluid Mechanics*, 702, 126–156. <https://doi.org/10.1017/jfm.2012.165>
- Sole, A. J., Mair, D. W. F., Nienow, P. W., Bartholomew, I. D., King, M. A., Burke, M. J., & Joughin, I. (2011). Seasonal speedup of a Greenland marine-terminating outlet glacier forced by surface melt-induced changes in subglacial hydrology. *Journal of Geophysical Research: Earth Surface*, 16, F03014. <https://doi.org/10.1029/2010JF001948>
- Sole, A. J., Nienow, P., Bartholomew, I., Mair, D., Cowton, T., Tedstone, A., & King, M. A. (2013). Winter motion mediates dynamic response of the Greenland Ice Sheet to warmer summers. *Geophysical Research Letters*, 40, 3940–3944. <https://doi.org/10.1002/grl.50764>
- Steffen, K., Box, J. E., & Abdalati, W. (1996). Greenland climate network: GC-net. Glaciers, Ice Sheets and Volcanoes: A Tribute to Mark F. Meier (Vol. special report 96-27). CRREL.
- Stevens, L. A., Behn, M. D., Das, S. B., Joughin, I., Noël, B. P. Y., van den Broeke, M. R., & Herring, T. (2016). Greenland Ice Sheet flow response to runoff variability. *Geophysical Research Letters*, 43, 11,295–11,303. <https://doi.org/10.1002/2016GL070414>
- Stevens, L. A., Behn, M. D., McGuire, J. J., Das, S. B., Joughin, I., Herring, T., et al. (2015). Greenland supraglacial lake drainages triggered by hydrologically induced basal slip. *Nature*, 522(7554), 73–76. <https://doi.org/10.1038/nature14480>
- Stroeve, J. C., Box, J. E., & Haran, T. (2006). Evaluation of the MODIS (MOD10A1) daily snow albedo product over the Greenland ice sheet. *Remote Sensing of Environment*, 105(2), 155–171. <https://doi.org/10.1016/j.rse.2006.06.009>
- Sugiyama, S., & Gudmundsson, H. (2004). Short-term variations in glacier flow controlled by subglacial water pressure at Lauteraargletscher, Bernese Alps, Switzerland. *Journal of Glaciology*, 50(170), 353–362. <https://doi.org/10.3189/172756504781829846>
- Sundal, A. V., Shepherd, A., Nienow, P., Hanna, E., Palmer, S., & Huybrechts, P. (2011). Melt-induced speed-up of Greenland ice sheet offset by efficient subglacial drainage. *Nature*, 469(7331), 521–524. <https://doi.org/10.1038/nature09740>
- Tedesco, M., Willis, I. C., Hoffman, M. J., Banwell, A. F., Alexander, P., & Arnold, N. S. (2013). Ice dynamic response to two modes of surface lake drainage on the Greenland ice sheet. *Environmental Research Letters*, 8(3), 034007. <https://doi.org/10.1088/1748-9326/8/3/034007>
- Tedstone, A. J., Nienow, P. W., Gourmelen, N., Dehecq, A., Goldberg, D., & Hanna, E. (2015). Decadal slowdown of a land-terminating sector of the Greenland Ice Sheet despite warming. *Nature*, 526(7575), 692–695. <https://doi.org/10.1038/nature15722>
- Tedstone, A. J., Nienow, P. W., Sole, A. J., Mair, D. W. F., Cowton, T. R., Bartholomew, I. D., & King, M. A. (2013). Greenland ice sheet motion insensitive to exceptional meltwater forcing. *Proceedings of the National Academy of Sciences*, 110(49), 19,719–19,724. <https://doi.org/10.1073/pnas.1315843110>



- Truffer, M., Echelmeyer, K. A., & Harrison, W. D. (2001). Implications of till deformation on glacier dynamics. *Journal of Glaciology*, 47(156), 123–134. <https://doi.org/10.3189/172756501781832449>
- van de Wal, R. S. W., Smeets, C. J. P. P., Boot, W., Stoffelen, M., van Kampen, R., Doyle, S. H., et al. (2015). Self-regulation of ice flow varies across the ablation area in south-west Greenland. *The Cryosphere*, 9(2), 603–611. <https://doi.org/10.5194/tc-9-603-2015>
- van de Wal, van de, R. S. W., Boot, W., van den Broeke, M. R., Smeets, C. J. P. P., Reijmer, C. H., et al. (2008). Large and rapid melt-induced velocity changes in the ablation zone of the Greenland Ice Sheet. *Science*, 321(5885), 111–113. <https://doi.org/10.1126/science.1158540>
- Walter, F., Chaput, J., & Lüthi, M. P. (2014). Thick sediments beneath Greenland's ablation zone and their potential role in future ice sheet dynamics. *Geology*, 42(6), 487–490. <https://doi.org/10.1130/G35492.1>
- Werder, M. A. (2016). The hydrology of subglacial overdeepenings: A new supercooling threshold formula. *Geophysical Research Letters*, 43, 2045–2052. <https://doi.org/10.1002/2015GL067542>
- Werder, M. A., & Funk, M. (2009). Dye tracing a jökulhlaup: II. Testing a jökulhlaup model against flow speeds inferred from measurements. *Journal of Glaciology*, 55(193), 899–908. <https://doi.org/10.3189/002214309790152375>
- Williamson, A. G., Arnold, N. S., Banwell, A. F., & Willis, I. C. (2017). A Fully Automated Supraglacial lake area and volume Tracking ("FAST") algorithm: Development and application using MODIS imagery of West Greenland. *Remote Sensing of Environment*, 196, 113–133. <https://doi.org/10.1016/j.rse.2017.04.032>
- Wright, P. J., Harper, J. T., Humphrey, N. F., & Meierbachtol, T. W. (2016). Measured basal water pressure variability of the western Greenland Ice Sheet: Implications for hydraulic potential. *Journal of Geophysical Research: Earth Surface*, 121, 1134–1147. <https://doi.org/10.1002/2016JF003819>
- Zwally, H. J., Abdalati, W., Herring, T., Larson, K., Saba, J., & Steffen, K. (2002). Surface melt-induced acceleration of Greenland ice-sheet flow. *Science*, 297(5579), 218–222. <https://doi.org/10.1126/science.1072708>